Unilateral loss of *recql4* function in *Xenopus laevis* tadpoles leads to ipsilateral ablation of the forelimb, hypoplastic Meckel's cartilage and vascular defects.

Caroline W. Beck[1], Matthew Reily-Bell[1,2] and Louise S. Bicknell[2]

1. Department of Zoology, University of Otago, Dunedin, New Zealand.
2. Department of Biochemistry, University of Otago, Dunedin, New Zealand.

Correspondence to: Associate Professor Caroline Beck: caroline.beck@otago.ac.nz

Abstract

RECQL4 encodes a RecQ helicase, one of a family of DNA unwinding enzymes with roles in DNA replication, double strand break repair and genomic stability. Pathogenic variants in *RECQL4* are clinically associated with three rare autosomal recessive conditions: Rothmund-Thomson Syndrome type II, Baller-Gerold Syndrome and RAPADILINO syndrome. These three syndromes show overlapping growth retardation, low bone density and skeletal defects affecting the arms and hands. Here, we take advantage of the ability to generate one-sided CRISPR knockdowns of *recql4* in *Xenopus laevis* tadpoles. Tadpoles develop normally until feeding starts, after which growth slows on the edited side leading to a curved posture, smaller eyes (micropthalmia) and reduced head size (microcephaly). Forelimb buds fail to develop, leading to complete absense of the forelimb on the edited side. Additionally, Meckel's cartilage (lower jaw) ossification is absent or reduced and the hyoid cartilage is smaller, but this is not due to deficiencies in cranial neural crest migration on the edited side. Knockdown of *recql4* also results in hypoplastic vasculature, with reduced branching from the aorta on the edited side. Taken together, our results clearly show the utility of unilateral CRISPR editing in *Xenopus* for understanding the specific phenotypic developmental effects of mutations affecting cell proliferation.

Keywords: *Xenopus laevis*, CRISPR, recql4, Meckel's cartilage, limbs, amelia, aortic branching, subclavian artery.

Introduction

Many developmental syndromes result from genetic alterations that disrupt timely and accurate DNA replication and DNA repair (Ichikawa *et al.*, 2002, Hoki *et al.*, 2003, Mann *et al.*, 2005, Bohr, 2008, Siitonen *et al.*, 2009, Larsen & Hickson, 2013, Croteau *et al.*, 2014, Smeets *et al.*, 2014, Lu *et al.*, 2015, Kaiser *et al.*, 2017, Castillo-Tandazo *et al.*, 2019, Bellelli & Boulton, 2021, Luong & Bernstein, 2021). RECQL4 belongs to a family of DNA helicases and has been shown to be required for DNA replication in *Xenopus laevis egg extracts* (Sangrithi *et al.*, 2005). Additionally, RECQL4 stabilizes and repairs replication forks and plays a role in repairing double stranded DNA breaks, (Singh *et al.*, 2010, Lu *et al.*, 2017, Luong & Bernstein, 2021). In humans, biallelic loss of function variants of *RECQL4* have been associated with three rare genetic conditions (RECQL4 syndromes): Rothmund Thomson syndrome (RTS) (Kitao *et al.*, 1999), Baller Gerald syndrome (BGS) (Van Maldergem *et al.*, 2006), and RAPADILINO syndrome (Siitonen *et al.*, 2003). While RAPADILINO syndrome mainly results from a single *RECQL4* variant more common in the Finnish population, BGS and RTS are genetically heterogeneous. All three RECQL4 syndromes show core overlapping phenotypes of growth retardation (leading to proportional short stature), radial ray defects in upper limbs (especially loss of thumbs), and osteopenia (low bone density) (Siitonen *et al.*, 2009, Luong & Bernstein, 2021). Additional phenotypes common in RTS type II are poikiloderma, a skin disorder shared with Bloom syndrome, and predisposition to osteosarcoma (Kitao *et al.*, 1999, Wang *et al.*, 2003). More recently, variants have been associated with myelodysplastic syndrome in multiple generations of a single family, although no functional experiments to test the missense variants were undertaken (Jiang *et al.*, 2023). Whether there are truly clinically distinct disorders caused by the disruption of the same gene rather than just very broad and heterogeneous clinical presentations is debated, (Van Maldergem *et al.*, 2016, Martins *et al.*, 2023) especially as the number of patients increase and genetic testing expands.

RECQL4 is a member of the RecQ helicase gene family. While prokaryotes and yeast contain only one RecQ gene, in humans and *Xenopus*, there are five: *RECQL, BLM/RECQL2, WRN/RECQL3, RECQL4 and RECQL5*. The proteins produced by these

genes all function in genome maintenance and stability and are often referred to as "guardians of the genome" (Hickson, 2003, Bohr, 2008, Larsen & Hickson, 2013, Croteau *et al.*, 2014). In addition to *RECQL4*, developmental syndromes have been attributed to genetic impairment of *RECQL* (RECON syndrome), *WRN* (Werner syndrome) and *BLM* (Bloom syndrome) (Abu-Libdeh *et al.*, 2022) While sharing many phenotypic similarities such as cancer predisposition and premature aging, RECQL4-associated syndromes are unique among the RECQ helicase family for the strong presence of skeletal abnormalities (Arora *et al.*, 2014, Oshima *et al.*, 2017, Abu-Libdeh *et al.*, 2022).

More than 100 *RECQL4* pathogenic variants have been reported, with most either nonsense or frameshift variants predicted to results in either null alleles (due to premature termination codons triggering nonsense-mediated decay pathways) or truncated proteins that would disrupt the helicase domain (Siitonen *et al.*, 2009, Castillo-Tandazo *et al.*, 2021). The C-terminal region of RECQL4 (RQC) is also known to be essential for activity (Mojumdar *et al.*, 2017) and the most common variant associated with BGS is in this region (Luong & Bernstein, 2021).

The exact mechanisms by which *RECQL4* variants cause the broad range of observed phenotypes are yet to be elucidated and several animal models have been developed. *Drosophila melanogaster* homozygous for null *recql4* mutations are lethal, and helicase-dead Recql4 does not complement this, suggesting that the helicase activity is critical for viability (Capp *et al.*, 2009). Similarly, deletion of all or part of the helicase domain in mice results in embryonic lethality (Hoki *et al.*, 2003, Smeets *et al.*, 2014). However, deletion of exons 5-8, which covers part of the N-terminal SLD-2 like DNA replication initiation domain of Recql4, also causes early embryonic lethality, even though the helicase domain (exons 8-14) is intact (Ichikawa *et al.*, 2002). A viable mouse model replicating the human skin and skeletal phenotypes was made by replacing exons 9-13 with a mini-gene cassette harboring termination codons, which created truncated *Recql4* transcripts (Mann *et al.*, 2005). Additionally, a substitution designed to remove the ATPase required for helicase function (K525A) did not cause adverse developmental effects in mice (Castillo-Tandazo *et al.*, 2019). There may be differences in expression

of RECQL4 that explain these different outcomes in mice and humans. Conditional mouse *recql4* mutants affecting the limb bud mesenchyme (Prx1-Cre) were viable and replicated limb skeletal defects seen in patients (Lu *et al.*, 2015).

In order to determine how loss of function of RECQL4 leads to specific developmental skeletal phenotypes in humans, such as short stature and limb defects, we turned to the model organism *Xenopus laevis*. *Xenopus* species are increasingly being used to model human genetic disease due to a high level of genetic conservation, ease of CRISPR/Cas9 editing, and well-characterized and observable development which occurs externally (reviewed in Willsey *et al.*, 2024). Additionally, it is possible to generate embryos and tadpoles that are edited only on one side of the body, by targeting CRISPR reagents to one cell of the two-cell stage embryo (Willsey *et al.*, 2021). Here, we take advantage of this to generate one-sided CRISPR/cas9 edited models of RECQL4 syndromes, in which the unedited side acts as an internal control for the phenotype. Edited tadpoles show ipsilateral phenotypes of reduced growth, absence of forelimb (and more rarely hindlimb) development, and specific craniofacial cartilage defects, all in keeping with, but more severe than, the phenotypes observed in humans. Intriguingly, we also observed hypoplastic aorta and failure to form the subclavian arterial branch on the edited side, which has not been reported previously. Our work shows the utility of *Xenopus* one-sided CRISPants to model disorders of growth caused by pathogenic variants in genes associated with replication, helping to explain how loss of function leads specific developmental phenotypes.

Methods

Animal ethics.

Xenopus laevis adults were held under University of Otago Animal Ethics Committee animal use procedure AUP-22-24, and embryos were produced according to AUP-22-12. CRISPR modification with *recql4* sgRNAs was approved and carried out according to AUP-25-04.

Production of one-sided recql4 CRISPants.

119 Adult female *Xenopus laevis* were induced to lay eggs by injection of 500 IU Chorulon
120 (HCG) per 75 g bodyweight, into the dorsal lymph sac. After 16 hours, females were
121 transferred into 1 x Marc's modified ringers (MMR: 10 mM NaCl, 0.1 mM $MgSO_4.6H_2O$,
122 0.2 mM $CaCl_2$, 0.5 mM HEPES, 10 μM EDTA, pH 7.8), from which eggs were collected
123 for *in vitro* fertilisation. Jelly coats were removed from embryos after 20 minutes by
124 gentle swirling in 2% L-Cysteine (pH 7.9) and rinsing 3 times in 1 x MMR.

125 Unique sgRNA sequences targeting *X. laevis recql4.L* (RefSeq: NM_001095713) were
126 designed using ChopChop v3 (Labun *et al.*, 2019). InDelphi (Shen *et al.*, 2018) was
127 used to predict editing efficiency in genomic context and to select guides predicted to
128 cause a dominant frameshift mutation (Figure 1, Table 1). The EnGen sgRNA oligo
129 designer v1.12.1 tool (NEB) was used to generate 55 bp oligonucleotides which were
130 synthesized by Integrated DNA Technologies (IDT). An EnGen Cas9 sgRNA kit (NEB)
131 was used to generate sgRNA by *in vitro* transcription. sgRNA were purified using a
132 Monarch RNA purification kit (NEB) and eluted into 30 μL pyrogen free water before
133 storing as 3μL aliquots at -70°C. sgRNA were loaded onto Cas9-NLS (EnGen, *S.*
134 *pyogenes*, NEB) as described in (Chapman *et al.*, 2022). Synthetic capped mRNA for
135 nGFP was prepared using an SP6 mMessage mMachine kit (Invitrogen) and added to
136 the injection mix, in order to track injection side. Two-cell stage embryos were
137 transferred into 5% Ficoll 400 in 1 x MMR and placed in a well cut into a 2% agar lined
138 50 mm petri dish for injection. Cas9/sgRNA plus nGFP mRNA, or just the mRNA, were
139 backloaded into a glass capillary needle (Drummond) pulled to a fine point using a
140 Sutter P92 needle puller and filled with light paraffin oil. 10 nl was injected into one cell
141 using a Nanoject III micropipette (Drummond) held with an MM3 micromanipulator. After
142 2-3 hours, embryos were transferred into 2.5% Ficoll in 0.1 x MMR and incubated at
143 23°C overnight.

144 Stage 25 neurula embryos were transferred into 0.1 x MMR and examined under
145 epifluorescence to determine the location of the injection. Embryos with clearly left or
146 right sided GFP were sorted and retained for phenotyping.

147 **Genotyping and editing analysis of CRISPants.**

148 For cohort genotyping, embryos with half green staining not tidily localised on the left or
149 right side were randomly selected and collected into 0.2 μL PCR tube strips. Any liquid
150 was removed and replaced with 150 μL of 5% Chelex 100 beads (Bio-Rad) suspended
151 in Tris/EDTA buffer, pH 8.0. Each sample was homogenised by pipetting and 30 μg of
152 Proteinase K (Sigma) was mixed in before incubating at 65 °C for 4 hours. Proteinase K
153 was then inactivated by heating for 15 minutes at 95 °C. PCR primers around the
154 editing site were designed using ChopChop v3 (Labun *et al.*, 2019) (Table) and 1 μL of
155 extracted DNA was PCR amplified for 35 cycles with MiFi mix (Bioline). The resulting
156 amplicon was cleaned using ExoSapIT (Applied Biosystems) and Sanger sequenced
157 (Genetics Analysis Service, University of Otago). Sequence traces were deconvoluted
158 by comparing to control unedited samples using TIDE v2 (Tracking of InDels by
159 Decomposition) to confirm editing (Brinkman *et al.*, 2014).

160 **Table 1. sgRNA and predicted editing**

Short guide RNA	**Sequence (PAM)**	**InDelphi predictions**			
		Frameshift frequency	Microhomology strength	Precision	Main InDels
sgRNA rank 8	GGATGTCGGCTGCGGAACGC**CGG**	94.8%	1.11	0.54	-8, -7, -5 bp
sgRNA rank 10	GATATCGCAGCTTCCGGTCG**GGG**	85.7%	1.32	0.58	-4, -5, -7 bp

161

162 **Table 2. Primers for amplification and sequencing**

Short guide RNA	**Forward primer**	**Reverse primer**	**Amplicon (bp)**
sgRNA rank 8	GAAATGATGGGTAACGAACC	TCTCAAAGTTCTTGGGCATA	385
sgRNA rank 10	GTACACCAAGGCATCATTTG	TTTGCCCATTCCTGTTGATA	839

163

164 **Phenotyping of unilateral CRISPants.**

165 Tadpoles were raised at 23°C in 10 mm petri dishes containing 0.1 x MMR until NF
166 stage 47 (Nieuwkoop & Faber, 1994). They were then fed with 100 μL of fresh spirulina
167 slurry and allowed to clear the dish overnight before moving to 1 L tanks and daily
168 spirulina feeding. At stage 48/49 they were moved to tanks in a recirculating aquarium
169 (Marine Biotech XR1) containing carbon filtered tap water, at a density of 25 tadpoles

170 per litre. Tadpoles were fed daily with a slurry of spirulina powder with a small amount of
171 ground adult frog pellets and recirculation turned off for two hours after each feed.

172 Tadpoles were anaesthetised twice briefly using 1/4000 v/v MS222 (Sigma) to observe
173 development and take photographs. At stage 50 (approx. two weeks) the presence or
174 absence of each limb bud was noted. At three weeks of age, 10 tadpoles per group
175 were individually photographed on agar-lined plates using a Leica MZ FLIII
176 stereomicroscope fitted with a Leica DFC320 camera and software. They were
177 illuminated from underneath with an A4 LED light box (Huion) and from the sides using
178 a swan neck light. FiJi image analysis (Schindelin *et al.*, 2012) was used to obtain a
179 quantification of left and right eye size and head size. Tadpoles were then recovered in
180 fresh tanks with gentle air bubbling for 1 hour and returned to the aquarium. Every 3
181 days, tadpoles that had reached stage NF 58, defined by the hatching of the forelimbs
182 from their pockets, were euthanised in 0.1% buffered benzocaine (Sigma), rinsed with
183 0.1 x MMR and fixed in 4% formaldehyde in phosphate buffered saline (PBS, Oxoid).
184 Following fixation overnight, tails were removed and photographs taken of each tadpole.

185 Bone and cartilage staining followed the method of (Newman & Dumont, 1983) with
186 modifications as in (Jones *et al.*, 2013). Briefly, fixed tadpoles were eviscerated in PBS
187 and bleached to remove skin pigmentation using 6% H_2O_2 in PBS. Alcian blue (0.01% in
188 40% acetic acid and 60% ethanol) was used to stain cartilage overnight, then destained
189 in 70% ethanol. Tadpoles were then soaked in 1% KOH to clear the muscle tissues
190 before staining the bone with alizarin red S (0.01% w/v in 1% KOH). Tadpoles were
191 destained in 1% KOH and then mounted in 50% glycerol/50% ethanol for photography.
192 Adobe Photoshop 2025 was used to prepare figures.

193 **In situ hybridisation.**

194 Whole mount colorimetric *in situ* hybridisation of stage 19 *recql4* half CRISPants was
195 carried out as in Beck et al 1998 (Beck & Slack, 1998). Digoxygenin-UTP labelled
196 antisense probes were visualised using anti-DIG Fab fragments conjugated to alkaline
197 phosphatase followed by enzymatic conversion of NBT/BCIP (Invitrogen) to generate a
198 dark blue precipitate. Embryos were bleached with 5% H_2O_2 post fixation.

199 **Table 3. Primers used to generate ISH antisense probes.**

Gene	Forward primer	Reverse primer	Amplicon size
Twist.S	ACCTTCTCCTTATTGTGCC	TGCTGTTAGTGAGATGCAG	533 bp
Snai2.L (xslug)	TTAAGGGACCGTTACTTGT	CATACTGCAATCTAATGTGC	851 bp
*Sox9.S**	CCGAACTCTCTTCTCC	CCTCTGTGTTGCAAGTTC	1608 bp
Sox10.L	TCAGTGAAGTTAACAGGCACCA	TTGCATTCCCTTCCCCCATC	1603 bp

200 * according to Jones, 2013 (Jones *et al.*, 2013).

201 **Graphing and statistical analysis.**

202 Data were graphed using GraphPad Prism v10.4.0. Quantitative data were first tested
203 for normal distribution using the Shapiro-Wilk test, with appropriate selection of non-
204 parametric tests for non-normal data.

205 Results

206 **Unilateral knockdown of *recql4* results in smaller head and eye size on the edited**
207 **side.**

208 Injection of cas9, *recql4* sgRNA8 or 10, and mRNA for nGFP into one cell at the 2-cell
209 stage resulted in efficient editing for both sgRNAs in samples arbitrarily chosen 18 hours
210 after injection (Figure 1B). The one cell injections resulted in a sharp left-right
211 expression boundary of GFP in 60-70% of cases, clearly seen at neurula stages (Figure
212 2A, A'). Using the co-injected transient GFP expression, embryos were sorted into clear
213 left and clear right-sided cohorts and raised to tadpole stages. No obvious differences
214 were observed at 5 days of age when feeding commenced. By three weeks of
215 development, tadpoles have reached stage 50-52. Differences in the head and eye size
216 on the side with *recql4* CRISPR knockdown with both sgRNA were clear in most
217 individuals (Figure 2 B-D; Figure S1; Table S1). Head size, estimated by measuring the
218 area either side of the midline from dorsal view photographs, was on average 1.4-fold
219 (sgRNA 8) or 1.2-fold (sgRNA10) larger on the uninjected side of right-sided CRISPants
220 (Figure 2). In left-sided CRISPants, head size was 1.4-fold (sgRNA8) and 1.3-fold
221 (sgRNA10) larger on the uninjected side. Control tadpoles (only injected with GFP)
222 showed no difference between left and right sides and were closest in size to the wild

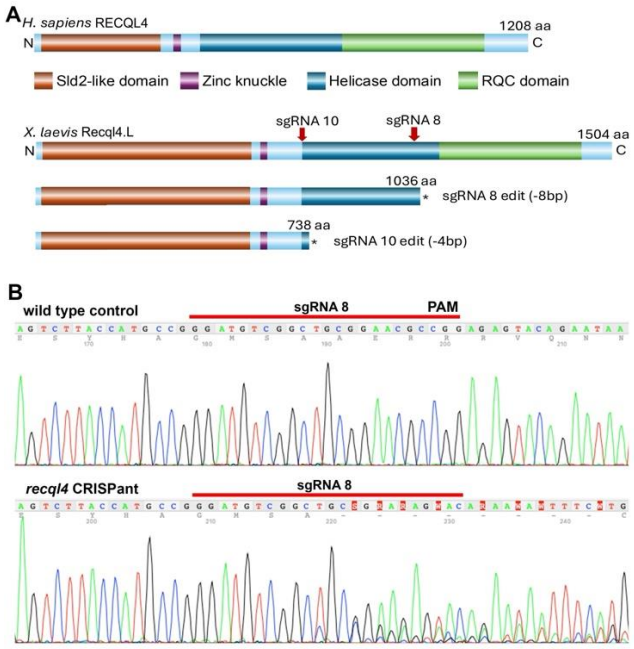

Figure 1. Schematic of *H. sapiens* and *X. laevis* RECQL4 proteins and CRISPR sgRNAs. **A)** Protein domain structure for human RECQL4 and *X. laevis* Recql4, red arrows indicate sgRNA target positions. Asterisk indicates premature stop codon. Both guides efficiently introduce truncating frameshifts: sgRNA 8 generates predominantly 8 bp deletions and sgRNA 10 has 4 bp deletions, both introduce a downstream stop codon in the helicase domain. **B)** Example of sgRNA8 editing, Sanger sequence traces from control wild type and sgRNA8 CRISPant. Guide sequence is indicated by red line.

type halves. Taken together, this data indicates that *Recql4* knockdown limits growth of the tadpole head to 70-80% of normal size (Figure 2E).

Similarly, eye size (estimated as the area of an ellipse covering the retina from the same photographs) was often noted to be smaller on the CRISPant side (Figure 2, Figure S1). For right-sided CRISPants, eye area was 1.6-fold (sgRNA8) and 1.3-fold (sgRNA10) larger on the wildtype side. For left-sided CRISPants, eye area was 1.2-fold larger on the wild type side for sgRNA8 and 1.7-fold larger for sgRNA10. Knockdown of *recql4* therefore also results in smaller size eyes, or micropthalmia (Figure 2F).

Forelimb development requires Recql4

NF58 tadpoles from the sgRNA 8 cohorts were pooled and examined for cartilage and skeletal defects. At stage NF58, the forelimbs have been released from the flap of skin under which they develop and can be observed by eye for the first time (Figure 3,

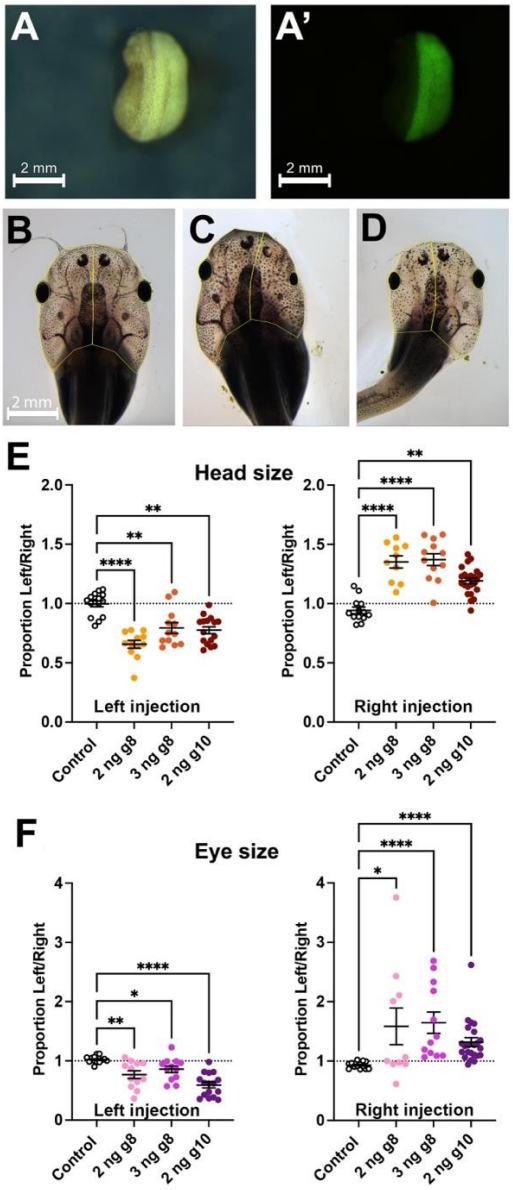

Figure 2: Unilateral knockdown of *recql4* results in smaller head and eye size on the edited side. A) Example of bright field and **A'**) fluorescence view of neurula embryo, dorsal view, anterior uppermost. Embryo was injected on the right side at the two-cell stage, GFP can be seen only on the right side of the midline. **B-D)** examples of tadpoles at 3 weeks, yellow outlines show the regions of interest (ROI) used to measure area of head and eye on left and right sides using FiJi. Scale bar in B applies to all panels. **B)** Control, injected with GFP mRNA only on the left side. **C)** Tadpole from the group injected with 2 ng *recql4* sgRNA 8 (g8) and nGFP mRNA on right, and **D)** on left. **E, F)** Scatter plots showing the proportions of left vs. right head (E) or eye (F) area. Line indicates mean ± SEM. Dotted line denotes no difference between the two sides. *Recql4* injected groups are compared to the control (only injected with GFP mRNA) using Kruskal Wallis tests with Dunn's post-hoc comparisons. Sample sizes are: GFP only controls: left N=15, right N=13, 2 ng g8 left N=12, right N=10, 3 ng g8 left N=12, right N=12, 2ng g10 left N=16, right N=23. Significantly different groups are indicated as p<0.05*, p<0.01**, p<0.001***, p<0.0001****. Raw data can be found in supplementary Tables S1-S10.

235 Figure S2, S3). The most frequently observed phenotype was a complete absence of
236 the forelimb on the side of the tadpole with *recql4* knocked down, seen in 30 of the 66
237 tadpoles scored at this stage. The forelimb has not failed to hatch from its pocket,
238 rather, is completely absent (Figure 3A). Tadpole swimming is often hampered by the
239 asymmetric nature of the head in *Recql4* unilateral CRISPants, which may lead to

240 slower growth (Supplementary video 1). Around half of the CRISPR tadpoles were
241 unable to reach stage NF58 several weeks after the last control (GFP) sibling was fixed,
242 indicating that developmental delay is an issue even in half CRISPants. We therefore
243 likely captured the weakest phenotypes, as they reached the goal stage of development
244 earlier. Unexpectedly, three individuals developed ectopic forelimbs on the edited side
245 (Figure 3B). In two cases, we saw mirror image duplicates. Figure 3B shows a right-
246 sided CRISPant with two perfectly formed forelimbs joined at the shoulder and with
247 mirror image polarity. In the third case, we saw a chaotic limb, the structure of which
248 was revealed by skeletal staining (Figure 3B, left CRISPant). The limb contained at least
249 three branches, each of which had one or more phalanges, but none of which was
250 correctly patterned. Overall, limb defects were almost exclusively found on the CRISPR
251 edited side of the tadpole, with only a single individual also lacking the contralateral
252 forelimb (Figure 3C).

253 Hindlimbs were also affected, although at a lower frequency, with 9/66 skeletal
254 preparations missing a hindlimb on the edited side (Figure 4, Table S11) (Figure 4 A, B,
255 D). A single ectopic hindlimb was observed (Figure 4C) with mirror image duplication of
256 the limb fused together at stylopod and zeugopod level by skin, and preaxial polydactyly
257 of the autopod with 8 digits clearly visible. Skeletal staining of this individual revealed a
258 single femur with duplicated tibia/fibula and two complete autopods, although both digit
259 1 copies had no ossification (Figure S4).

260 ***Recql4* unilateral CRISPants have craniofacial defects on the edited side.**

261 The skeletal preparations used to examine limb development also provided an
262 opportunity to observe craniofacial development and ossification. In a group of 16 right-
263 sided and 15 left-sided CRISPant tadpoles, defects in ossification of the Meckel's

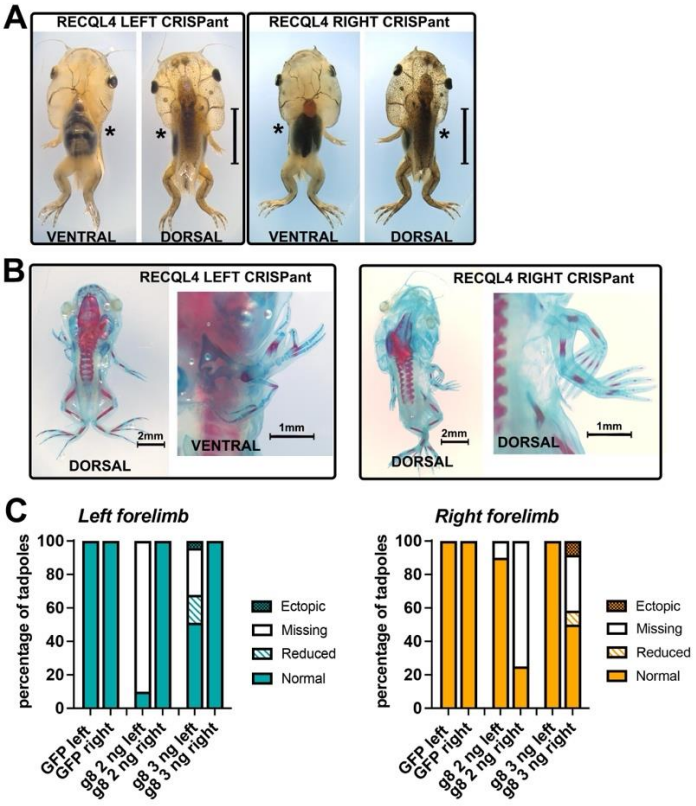

Figure 3: Forelimb development requires Recql4. A) Stage NF 58 tadpoles commonly lack a forelimb on the CRISPR edited side. Examples of left and right sided *Recql4* CRISPANT tadpoles, dorsal and ventral views. Missing forelimbs are indicated by an asterisk, scale bar is 5 mm. Tails have been removed to aid visualisation. **B)** Whole skeletal preparations of example stage NF 58 tadpoles where the edited side forelimb was not missing but instead was severely disrupted or duplicated, with ectopic structures present. Blue stain is cartilage (alcian blue) and red stain shows bone (alizarin red). The whole tadpole is shown in the left image and a zoomed view of the ectopic limb on the right, viewed from the side that best shows the limb elements. **C)** Stacked bar graphs showing observed frequency of forelimb phenotypes on left and right sides in half-CRISPant stage. Sample sizes according to treatment and injection side are: mRNA for nGFP only (GFP) left N=20, right = 14; *recql4* sgRNA 8 (g8) 2ng left N=10, right N=8; *recql4* g8 3ng left N=24, right N=24. Raw count data can be found in Table S12 and images in Figure S2.

cartilage were frequently observed on the edited side (Figure 5). These ranged from total lack of ossified bone (6/16 right-sided CRISPants, 4/15 left-sided CRISPants) to reduction or fragmentation of the ossified region (6/16 and 5/15 respectively) compared to the wild-type side (Figure 5A-C). This was clearly visible as reduced or absent alizarin red staining viewed from the ventral side. Other craniofacial structures were also affected, particularly the hyoid cartilage, which was often smaller on the edited side (9/16 right sided and 10/15 left sided CRISPants, Figure 5A, B, D).

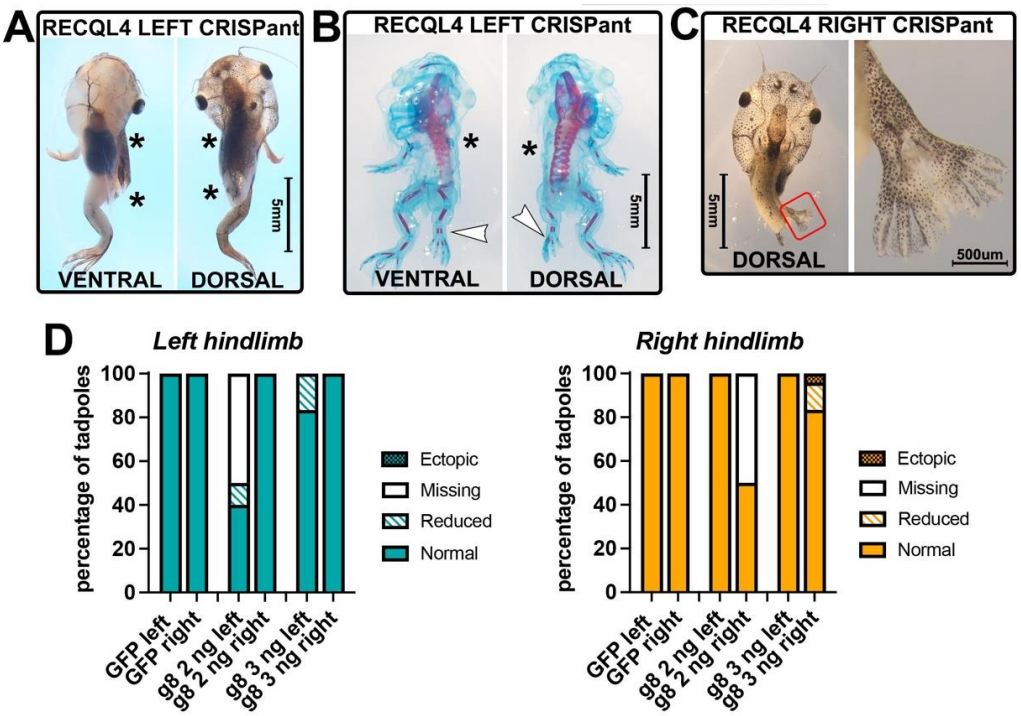

Figure 4: Hindlimbs are more resistant to loss of *Recql4* than forelimbs. A) Example of NF 58 stage tadpole where CRISPR knockdown of *recql4* on the left side has led to failure of the left hindlimb to develop as well as the forelimbs. Missing limbs are indicated by an asterisk. **B)** Skeletal preparation of NF58 tadpole showing example of a smaller hindlimb on the recql4 edited left side (white arrowhead). Bone and cartilage staining show that this limb is not missing any elements. This individual is also missing the left forelimb as indicated with an asterisk. **C)** A single example of an ectopic hindlimb found in the study is shown. This tadpole is stage NF55 and editing is on the right. Two limbs appear as a mirror image duplication (preaxial polydactyly) on the right side, and a single limb (partially obscured by the tail) on the left. Both forelimbs are present but cannot be seen due to the pre-hatching stage. **D)** Stacked bar graphs showing observed frequency of hindlimb phenotypes on left and right sides in half-CRISPant tadpoles. Sample sizes are: GFP right N=14; GFP left N=20; g8 2 ng right N=8; g8 2 ng left N=10; g8 3 ng left N=24; g8 3 ng right N=24. Count data is in Tables S13-16.

The cartilages of the head are built from the descendants of migrating cranial neural crest cells, which leave the dorsal neural tube in three streams during the neurula stages of development. Fate mapping experiments have shown that the most anterior of these, the mandibular stream, contributes to Meckel's cartilage (lower jaw), quadrate cartilage (upper jaw) and parts of the skull, with the central stream giving rise to the hyoid cartilage (Sadaghiani & Thiébaud, 1987). Craniofacial defects like these are often the result of aberrant migration of neural crest, and *Xenopus* is a well-established model to determine this (reviewed in (Dubey & Saint-Jeannet, 2017). To see if the defects were caused by failure of these cells to migrate correctly when *recql4* has been edited, we

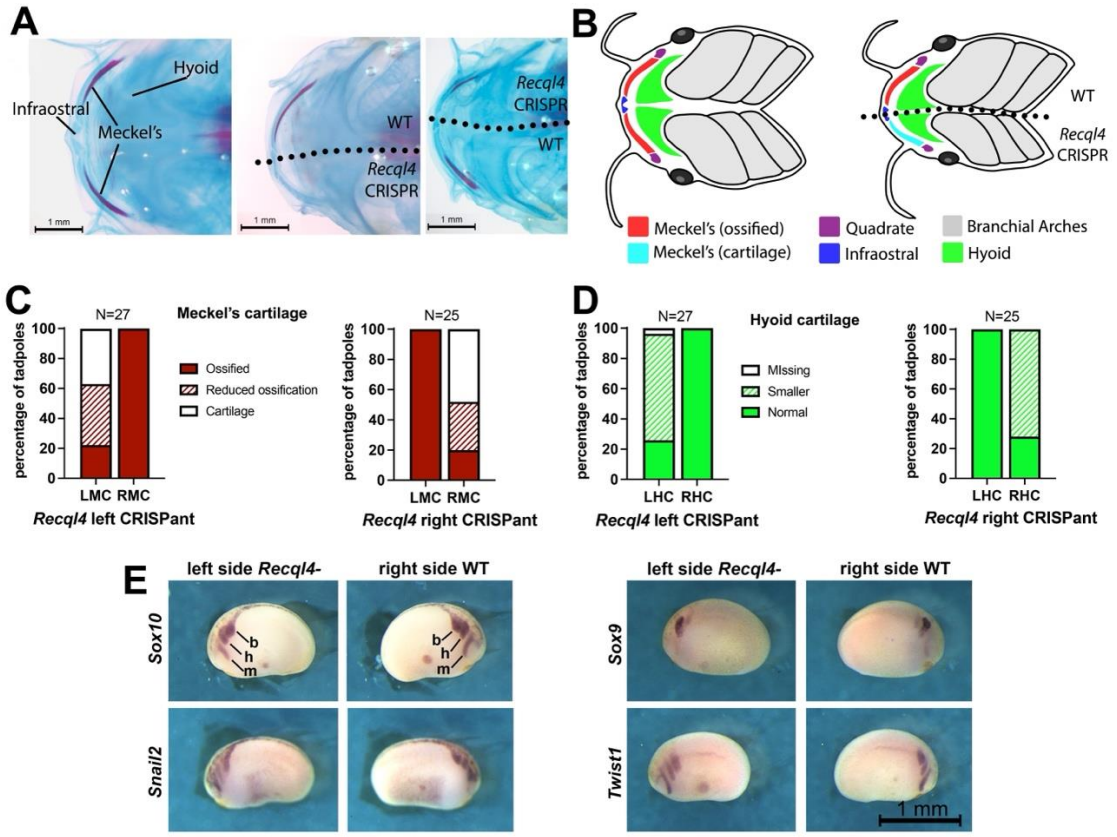

Figure 5: *Recql4* unilateral CRISPants have craniofacial defects on the edited side, but this does not arise from altered migration of cranial neural crest cells. A) Tadpole stage NF58 skeletal preparations, showing a ventral view of the jaw with cartilage stained blue and ossified bone stained red. Left image shows a control tadpole, centre shows a tadpole where *recql4* was knocked down on the left side (no ossification of Meckel's cartilage on injected side), and right shows a tadpole with *recql4* knockdown on the right side (reduced ossification of Meckel's on injected side. **B)** Diagram of control and left-sided CRISPant tadpole ventral craniofacial structures to show the positions of the cartilages. **C)** Stacked bar graph comparing the frequency of reduced or absent ossification of Meckel's cartilage on left (LMC) and right (RMC) in left (N=15) and right (N=16) sided unilateral CRISPants. **D)** Stacked bar graph comparing the frequency of smaller sized hyoid cartilage on left (LMC) and right (RMC) in left (N=15) and right (N=16) sided unilateral CRISPants. **E)** In situ hybridisation of early cranial neural crest markers in stage 19 unilateral *recql4* CRISPants (left side edited). The cranial neural crest cells migrate from the dorsal neural tube in three streams, the mandibular (m), hyoid (h) and branchial (b). The scale bar in the bottom right panel relates to all panels. Supporting data can be found in Figure S3.

examined the expression of four marker genes: *sox10, snail2, sox9* and *twist1* (Alfandari *et al.*, 2001, Aoki *et al.*, 2003, Lee & Saint-Jeannet, 2011) in unilateral *recql4* CRISPants (sgRNA8, Figure 5E). We saw no differences in the extent of migration or intensity of signal indicating that cranial neural crest migrates normally in the absence of

Recql4. These results suggest that the reduced size of the hyoid cartilage results from hypoplastic growth.

Forelimb buds fail to develop in the absence of Recql4, and vasculature of the head is hypoplastic with reduced branching.

To determine whether the anterior limb buds developed and then regressed, or just never developed in the absence of Recql4, we examined tadpoles at 4 weeks of development (Figure 6, Tables S11-S14). Forelimb buds were absent on the ipsilateral side in 87% of tadpoles: 13/16 left *recql4* CRISPants and 20/22 right *recql4* CRISPants (Figure 6A). The contralateral wild type forelimb was missing as well in 2/16 left CRISPants and 2/22 right CRISPants. Hindlimb defects less commonly observed, but still missing on the ipsilateral side of 20% of tadpoles. One left CRISPant was missing the ipsilateral hindlimb and two had hindlimbs that were developmentally delayed by two NF stages. 7/22 right CRISPants were missing the ipsilateral hindlimb bud (Figure 6A). These observations from an earlier timepoint in development support the conclusion that forelimb buds fail to develop in the absence of Recql4.

While scoring the limbs, we noticed that the vasculature was also altered in the ipsilateral head region, with the CRISPR side consistently having a narrower aorta. Additionally, some arteries that branch from the aorta were absent on the CRISPR side, particularly the subclavian artery (Figure 6B, Supplementary video 2, Supplementary video 3).

Discussion

Here we have used CRISPR/Cas9 editing to study the effects of depleting Recql4, using two sgRNAs in different positions to help further understand developmental consequences caused by frameshift variants in different parts of the *recql4* gene. Following injection of the two different sgRNAs, CRISPants showed concordant phenotypes, despite the difference in position of editing. In other animal models, different phenotypes have been observed depending on the variant position. For example, mouse models harbouring either p.Arg347* or p.G522fs variants showed different effects on the protein (weak expression of truncated protein versus no

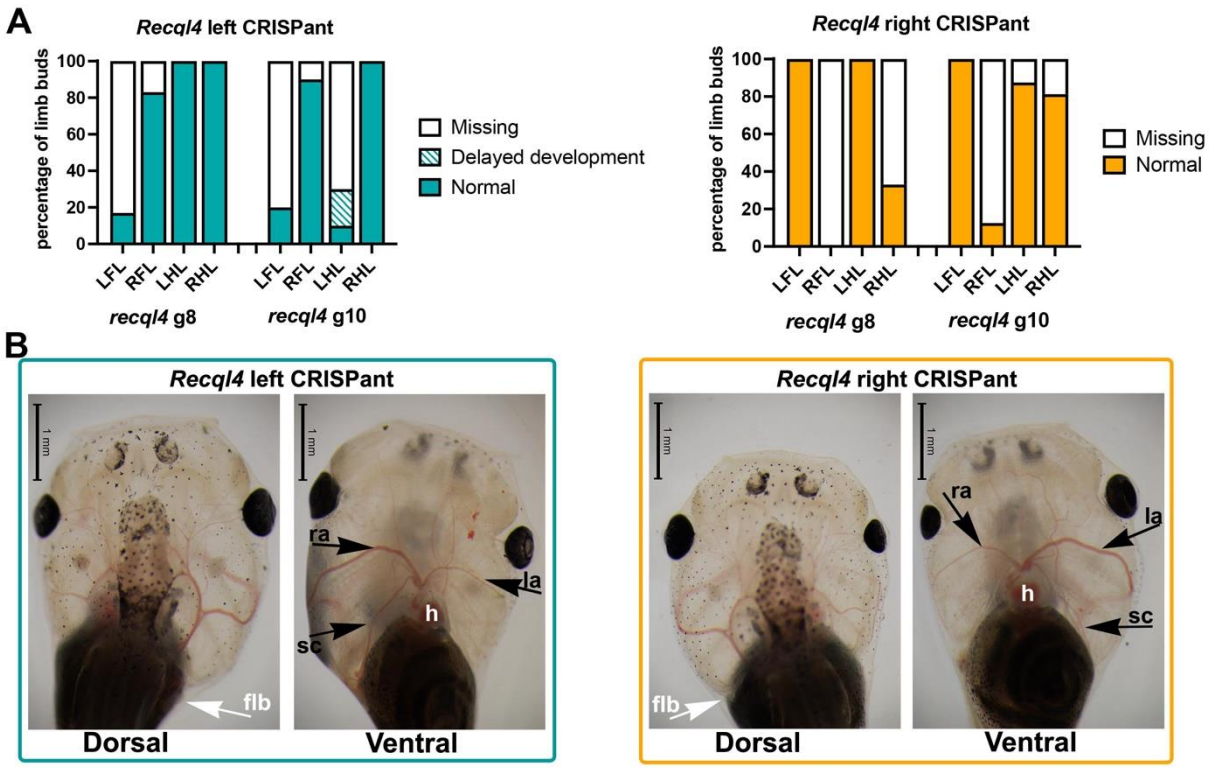

Figure 6: The forelimb bud fails to develop and vasculature of the head is reduced in the absense of Recql4. **A)** Stacked bar graphs showing observed frequency of forelimb absence or delayed development on left and right sides in half-CRISPant tadpoles at 4 weeks old (stages NF50-54). Sample sizes: sgRNA8: N=6 left and N=6 right CRISPants; sgRNA10: N=10 left and N=16 right CRISPants. **B)** Dorsal and ventral views of the head of typical unilateral CRISPant tadpoles at 4 weeks of development. The heart and vascular system can be clearly seen due to the natural transparency of the tadpole head.Labels: flb, forelimb bud; h, heart; ra, right aorta; la, left aorta; sc, subclavian artery. Raw data can be found in supplementary Tables S11-S14.

expression, respectively) and the p.Arg347* variant caused a more severe skeletal phenotypes (Castillo-Tandazo *et al.*, 2021). A missense variant which inactivates the helicase, p.K525A, showed no phenotype in a mouse model, although the skeletal system was not studied in detail (Castillo-Tandazo *et al.*, 2019). The majority of variants identified in humans have also not been characterised in a cellular system, so trying to establish genotype-phenotype patterns or design precise animal models remains difficult.

Translational effects of variants in the *recql4* gene appear to be complex in all models studied (Castillo-Tandazo *et al.*, 2019, Castillo-Tandazo *et al.*, 2021). While some variants that cause premature stop codons, through either nonsense or frameshift variants, result in little protein expression (likely through nonsense-mediated decay

pathways regulating the aberrant mRNA), others result in the production of a truncated protein, albeit at a reduced level (Castillo-Tandazo *et al.*, 2021). An unusual, evolutionarily conserved feature of the *recql4* genes is the significant number of very short introns. Exactly how these might impact mRNA quality surveillance and splicing has not been determined, but these likely play a role in the complexity of Recql4 translational products and levels when variants are present.

A strong advantage to our approach was to harness the unique left/right separation of the body plan which is present in *X. laevis* from the very first cell division. This enables targeting of CRISPR editing to one side of the body, with the co-injection of mRNA for nuclear GFP allows accurate sorting of embryos from neurula stages (24 hours from injection) into left and right CRISPants. Amplicon Sanger sequencing showed that both guides were efficient editors, resulting in around 50% of the genome overall, indicting that levels of editing on the targeted side are close to 100%. As demonstrated, this enabled an inbuilt control and thereby a more precise study of phenotypes caused by gene editing. The injected side of the CRISPant tadpoles had smaller heads and eyes. Growth defects, including short stature and/or microcephaly, are well established in human disorders associated with *RECQL4* (Wang & Plon, 1999, Van Maldergem *et al.*, 2007). Eyes are a highly proliferative tissue, and in other animal models where microcephaly has occurred, smaller eyes can also be present (Hempel *et al.*, 2016, Johnson *et al.*, 2024, Satou-Kobayashi *et al.*, 2024). Microphthalmia has only been noted in one individual with *RECQL4* variants (Yadav *et al.*, 2019) and so the observation that CRISPants have smaller eyes, is more likely a secondary consequence of overall reduced growth, rather than a distinct feature.

The skeletal defects caused by the editing aligned with the human cases of *RECQL4* and mouse skeletal models (Kitao *et al.*, 1999, Siitonen *et al.*, 2003, Piard *et al.*, 2015). Forelimbs were much more likely to be absent rather than hypoplastic, suggesting a failure early in limb development. The effect on hindlimbs was not as commonly observed, but similar in that the limb was more likely to be absent rather than reduced. This could either reflect the editing approach used, or insight into the underlying biology. While forelimbs develop on opposite sides of the trunk, hindlimb buds develop very

354 close together at the midline. Cell mixing across the midline due to this proximity could
355 therefore contribute some wild type cells to the edited limb mesenchyme, giving a
356 threshold amount of wildtype Recql4 on the edited sides. The forelimb buds are much
357 further apart, so cell mixing would be less likely. However, it is noteworthy that in
358 humans harbouring *RECQL4* variants, arms are also more often affected than legs and
359 feet. Radial ray defects are a specific grouping of skeletal anomalies affecting the
360 radius, radial carpal bones and thumb, arising from failures in limb bud mesoderm
361 growth and patterning, but there is not an equivalent grouping affecting legs and feet.
362 Forelimb absence in our CRISPants could be considered an extreme failure of limb bud
363 mesoderm growth and patterning.

364 In a few cases we did observe ectopic hind or forelimbs developing, resembling
365 complete mirror image polydactlyly caused by mis-expression of *shh* (Riddle *et al.*,
366 1993) or grafting of the zone of polarising activity ZPA (Honig & Summerbell, 1985) in
367 chickens. A duplicated thumb (preaxial polydactyly) has been reported in a single case
368 with *RECQL4* variants (Piard *et al.*, 2015). While this unexpected phenotype has been
369 observed in both *X. laevis* and humans, it is not clear how Recql4 knockdown could
370 lead to these diametrically opposed phenotypes of hypomorphic/missing limbs and
371 anterior-posterior limb duplications. Seemingly opposed phenotypes of limb hypoplasia
372 and limb duplication have also been observed to result from overexpression of the BMP
373 inhibitor Noggin1 at different developmental stages in inducible transgenic lines (Jones
374 *et al.*, 2013). These different observations further support that Recql4 must have
375 specific role(s) in skeletal development and potentially form a starting point to
376 understand the link between Recql4 function and developmental processes in the limb
377 bud.

378 We also observed some features unique to our CRISPant models. While some facial
379 dysmorphism is occasionally seen in *RECQL4*-associated individuals (Piard *et al.*,
380 2015), including micrognathia, we observed stronger phenotypes in our models. The
381 edited side of the head was smaller overall and often showed either reduced,
382 fragmented or a total lack of ossification. The ossification of Meckel's cartilage and the
383 size of the hyoid cartilage were particularly sensitive to loss of Recql4 – although for the

384 hyoid cartilage it was more likely reduced in the size than absent, which is different to
385 the forelimb and hindlimb consequences we observed. Using in situ hybridization, we
386 confirmed that this is not due to generalised neural crest migration defects, suggesting a
387 more specific effect on these structures caused by reduced or absent Recql4. Meckel's
388 cartilage is a conserved developmental feature of all jawed vertebrates, which acts as a
389 template for later forming jaw bones, but it has evolved a distinct role in mammals
390 whereby the proximal part ossifies and forms the malleus and incus, two of the three
391 middle ear bones (Svandova *et al.*, 2020). There are no reports of disruption to these
392 bones in the human *recql4* syndromes that we are aware of. It is also not clear whether
393 the lack of ossification in stage 58 tadpoles is a delay in the process or complete failure,
394 since tadpoles were not raised past this stage. Despite the differences in anatomy, the
395 observations of delayed or failed ossification in both the tadpole Meckel's cartilage (this
396 study) and the human patella (Wang & Plon, 1999) suggest a role for Recql4 in
397 endochondral ossification. Failure to ossify the patella also occurs in Meier-Gorlin
398 syndrome, a multigenic disorder that results in growth retardation due to impaired
399 replication licencing (Klingseisen & Jackson, 2011, de Munnik *et al.*, 2015).

400 Intriguingly, when checking the younger stage tadpoles to see if limb buds ever formed,
401 we observed absence of a major nearby blood vessel, likely the subclavian artery. No
402 vasculature abnormalities have been noted in human patients, although links between
403 angiogenesis (the formation of new blood vessels) and limb development are
404 highlighted by the dramatic teratogenic nature of the drug thalidomide (reviewed in
405 (Vargesson & Hootnick, 2017)). A failure to form both the forelimb bud and the
406 subclavian artery that supplies the forelimb may suggest a developmental co-
407 dependence. The timing of the formation of the *Xenopus* subclavian artery has not been
408 described, but in humans and mice it seems to only become established *after* the
409 initiation of limb bud development, (Rodríguez-Niedenführ *et al.*, 2001, Walls *et al.*,
410 2008). Alternatively, reduced aortic branching could result from interference with the
411 VEGF signalling that drives this process, or simply reflect the poor growth on the side of
412 the tadpole that has Recql4 knockdown. The aortic arch appeared consistently narrower
413 on the CRISPR side, suggesting the latter.

414 In conclusion, our model establishes single-sided genome editing as a useful approach
415 for studying developmental effects of reduced Recql4. Many phenotypes observed in
416 edited tadpoles align with both the human and mouse models, but we have also
417 observed unique abnormalities that could either point to *X. laevis* specific requirements
418 for Recql4, or broader effects caused by a developmental role for Recql4 that has not
419 yet been fully determined. The cellular roles for RECQL4 continue to be explored
420 (Ashraf *et al.*, 2025); such further insight may aid in deciphering these unique
421 phenotypes observed.

422 **Acknowledgements:**

423 We gratefully acknowledge funding from the Neurological Foundation of New Zealand
424 (PRG1732 to LSB, CB) We would like to thank Nikita Woodhead and her team for her
425 excellent care of the *Xenopus* colony.

426 **Author contributions:**

427 Experimental design, implementation and analysis CB, MRB. Animal ethics CB,
428 Manuscript writing CB, MRB, LSB.

429 **References:**

430 Abu-Libdeh B, Jhujh SS, Dhar S*, et al.* (2022) RECON syndrome is a genome instability disorder caused
431 by mutations in the DNA helicase RECQL1. *J Clin Invest* **132**: e147301.

432 Alfandari D, Cousin H, Gaultier A, Smith K, White JM, Darribère T & DeSimone DW (2001) Xenopus
433 ADAM 13 is a metalloprotease required for cranial neural crest-cell migration. *Curr Biol* **11**: 918-930.

434 Aoki Y, Saint-Germain N, Gyda M, Magner-Fink E, Lee YH, Credidio C & Saint-Jeannet JP (2003) Sox10
435 regulates the development of neural crest-derived melanocytes in Xenopus. *Dev Biol* **259**: 19-33.

436 Arora H, Chacon AH, Choudhary S, McLeod MP, Meshkov L, Nouri K & Izakovic J (2014) Bloom
437 syndrome. *Int J Dermatol* **53**: 798-802.

438 Ashraf R, Polasek-Sedlackova H, Marini V, Prochazkova J, Hasanova Z, Zacpalova M, Boudova M &
439 Krejci L (2025) RECQ4-MUS81 interaction contributes to telomere maintenance with implications to
440 Rothmund-Thomson syndrome. *Nature Communications* **16**: 1302.

441 Beck CW & Slack JM (1998) Analysis of the developing Xenopus tail bud reveals separate phases of
442 gene expression during determination and outgrowth. *Mech Dev* **72**: 41-52.

443 Bellelli R & Boulton SJ (2021) Spotlight on the Replisome: Aetiology of DNA Replication-Associated
444 Genetic Diseases. *Trends in Genetics* **37**: 317-336.

445 Bohr VA (2008) Rising from the RecQ-age: the role of human RecQ helicases in genome maintenance.
446 *Trends Biochem Sci* **33**: 609-620.

447 Brinkman EK, Chen T, Amendola M & van Steensel B (2014) Easy quantitative assessment of genome
448 editing by sequence trace decomposition. *Nucleic Acids Res* **42**: e168.

449 Capp C, Wu J & Hsieh TS (2009) Drosophila RecQ4 has a 3'-5' DNA helicase activity that is essential for
450 viability. *J Biol Chem* **284**: 30845-30852.

451 Castillo-Tandazo W, Frazier AE, Sims NA, Smeets MF & Walkley CR (2021) Rothmund-Thomson
452 Syndrome-Like RECQL4 Truncating Mutations Cause a Haploinsufficient Low-Bone-Mass Phenotype in
453 Mice. *Mol Cell Biol* **41**: e0059020.

454 Castillo-Tandazo W, Smeets MF, Murphy V, Liu R, Hodson C, Heierhorst J, Deans AJ & Walkley CR
455 (2019) ATP-dependent helicase activity is dispensable for the physiological functions of Recql4. *PLoS*
456 *genetics* **15**: e1008266.

457 Chapman PA, Gilbert CB, Devine TJ, Hudson DT, Ward J, Morgan XC & Beck CW (2022) Manipulating
458 the microbiome alters regenerative outcomes in Xenopus laevis tadpoles via lipopolysaccharide
459 signalling. *Wound Repair Regen* **30**: 636-651.

460 Croteau DL, Popuri V, Opresko PL & Bohr VA (2014) Human RecQ helicases in DNA repair,
461 recombination, and replication. *Annu Rev Biochem* **83**: 519-552.

462 de Munnik SA, Hoefsloot EH, Roukema J, Schoots J, Knoers NV, Brunner HG, Jackson AP & Bongers
463 EM (2015) Meier-Gorlin syndrome. *Orphanet J Rare Dis* **10**: 114.

464 Dubey A & Saint-Jeannet JP (2017) Modeling human craniofacial disorders in Xenopus. *Curr Pathobiol*
465 *Rep* **5**: 79-92.

466 Hempel A, Pagnamenta AT, Blyth M*, et al.* (2016) Deletions and de novo mutations of SOX11 are
467 associated with a neurodevelopmental disorder with features of Coffin-Siris syndrome. *J Med Genet* **53**:
468 152-162.

469 Hickson ID (2003) RecQ helicases: caretakers of the genome. *Nature reviews Cancer* **3**: 169-178.

470 Hoki Y, Araki R, Fujimori A*, et al.* (2003) Growth retardation and skin abnormalities of the Recql4 -deficient
471 mouse. *Human Molecular Genetics* **12**: 2293-2299.

472 Honig LS & Summerbell D (1985) Maps of strength of positional signalling activity in the developing chick
473 wing bud. *J Embryol Exp Morphol* **87**: 163-174.

474 Ichikawa K, Noda T & Furuichi Y (2002) [Preparation of the gene targeted knockout mice for human
475 premature aging diseases, Werner syndrome, and Rothmund-Thomson syndrome caused by the
476 mutation of DNA helicases]. *Nihon Yakurigaku Zasshi* **119**: 219-226.

477 Jiang C, Zhang H, Zhao C, Wang L, Hu X & Pan Z (2023) De novo myelodysplastic syndrome in a
478 Rothmund-Thomson Syndrome patient with novel pathogenic RECQL4 variants. *Blood Sci* **5**: 125-130.

479 Johnson HK, Wahl SE, Sesay F, Litovchick L & Dickinson AJ (2024) Dyrk1a is required for craniofacial
480 development in Xenopus laevis. *Dev Biol* **511**: 63-75.

481 Jones TE, Day RC & Beck CW (2013) Attenuation of bone morphogenetic protein signaling during
482 amphibian limb development results in the generation of stage-specific defects. *J Anat* **223**: 474-488.

483 Kaiser S, Sauer F & Kisker C (2017) The structural and functional characterization of human RecQ4
484 reveals insights into its helicase mechanism. *Nature Communications* **8**: 15907.

485 Kitao S, Shimamoto A, Goto M, Miller RW, Smithson WA, Lindor NM & Furuichi Y (1999) Mutations in
486 RECQL4 cause a subset of cases of Rothmund-Thomson syndrome. *Nat Genet* **22**: 82-84.

487 Klingseisen A & Jackson AP (2011) Mechanisms and pathways of growth failure in primordial dwarfism.
488 *Genes Dev* **25**: 2011-2024.

489 Labun K, Montague TG, Krause M, Torres Cleuren YN, Tjeldnes H & Valen E (2019) CHOPCHOP v3:
490 expanding the CRISPR web toolbox beyond genome editing. *Nucleic Acids Research* **47**: W171-W174.

491 Larsen NB & Hickson ID (2013) RecQ Helicases: Conserved Guardians of Genomic Integrity. *Adv Exp*
492 *Med Biol* **767**: 161-184.

493 Lee YH & Saint-Jeannet JP (2011) Sox9 function in craniofacial development and disease. *Genesis* **49**:
494 200-208.

495 Lu H, Shamanna RA, de Freitas JK*, et al.* (2017) Cell cycle-dependent phosphorylation regulates
496 RECQL4 pathway choice and ubiquitination in DNA double-strand break repair. *Nature Communications*
497 **8**: 2039.

498 Lu L, Harutyunyan K, Jin W*, et al.* (2015) RECQL4 Regulates p53 Function In Vivo During
499 Skeletogenesis. *J Bone Miner Res* **30**: 1077-1089.

500 Luong TT & Bernstein KA (2021) Role and Regulation of the RECQL4 Family during Genomic Integrity
501 Maintenance. *Genes (Basel)* **12**.

502 Mann MB, Hodges CA, Barnes E, Vogel H, Hassold TJ & Luo G (2005) Defective sister-chromatid
503 cohesion, aneuploidy and cancer predisposition in a mouse model of type II Rothmund–Thomson
504 syndrome. *Human Molecular Genetics* **14**: 813-825.

505 Martins DJ, Di Lazzaro Filho R, Bertola DR & Hoch NC (2023) Rothmund-Thomson syndrome, a disorder
506 far from solved. *Frontiers in Aging* **4**.

507 Mojumdar A, De March M, Marino F & Onesti S (2017) The Human RecQ4 Helicase Contains a
508 Functional RecQ C-terminal Region (RQC) That Is Essential for Activity. *J Biol Chem* **292**: 4176-4184.

509 Newman SM, Jr. & Dumont JN (1983) Thiosemicarbazide-induced osteolathyrism in metamorphosing
510 Xenopus laevis. *J Exp Zool* **225**: 411-421.

511 Nieuwkoop PD & Faber J (1994) *Normal Table of Xenopus laevis (Daudin): a systematical and*
512 *chronological survey of the development from the fertilized egg till the end of metamorphosis*. Garland
513 Publishing Inc, New York & London.

514 Oshima J, Sidorova JM & Monnat RJ, Jr. (2017) Werner syndrome: Clinical features, pathogenesis and
515 potential therapeutic interventions. *Ageing Res Rev* **33**: 105-114.

516 Piard J, Aral B, Vabres P*, et al.* (2015) Search for ReCQL4 mutations in 39 patients genotyped for
517 suspected Rothmund-Thomson/Baller-Gerold syndromes. *Clin Genet* **87**: 244-251.

518 Riddle RD, Johnson RL, Laufer E & Tabin C (1993) Sonic hedgehog mediates the polarizing activity of the
519 ZPA. *Cell* **75**: 1401-1416.

520 Rodríguez-Niedenführ M, Burton GJ, Deu J & Sañudo JR (2001) Development of the arterial pattern in
521 the upper limb of staged human embryos: normal development and anatomic variations. *J Anat* **199**: 407-
522 417.

523 Sadaghiani B & Thiébaud CH (1987) Neural crest development in the Xenopus laevis embryo, studied by
524 interspecific transplantation and scanning electron microscopy. *Developmental Biology* **124**: 91-110.

525 Sangrithi MN, Bernal JA, Madine M, Philpott A, Lee J, Dunphy WG & Venkitaraman AR (2005) Initiation of
526 DNA replication requires the RECQL4 protein mutated in Rothmund-Thomson syndrome. *Cell* **121**: 887-
527 898.

528 Satou-Kobayashi Y, Takahashi S, Haramoto Y, Asashima M & Taira M (2024) Zbtb11 interacts with Otx2
529 and patterns the anterior neuroectoderm in Xenopus. *PLOS ONE* **19**: e0293852.

530 Schindelin J, Arganda-Carreras I, Frise E*, et al.* (2012) Fiji: an open-source platform for biological-image
531 analysis. *Nature Methods* **9**: 676-682.

532 Shen MW, Arbab M, Hsu JY, Worstell D, Culbertson SJ, Krabbe O, Cassa CA, Liu DR, Gifford DK &
533 Sherwood RI (2018) Predictable and precise template-free CRISPR editing of pathogenic variants. *Nature*
534 **563**: 646-651.

535 Siitonen HA, Kopra O, Kääriäinen H, Haravuori H, Winter RM, Säämänen AM, Peltonen L & Kestilä M
536 (2003) Molecular defect of RAPADILINO syndrome expands the phenotype spectrum of RECQL
537 diseases. *Hum Mol Genet* **12**: 2837-2844.

538 Siitonen HA, Sotkasiira J, Biervliet M*, et al.* (2009) The mutation spectrum in RECQL4 diseases.
539 *European Journal of Human Genetics* **17**: 151-158.

540 Singh DK, Karmakar P, Aamann M, Schurman SH, May A, Croteau DL, Burks L, Plon SE & Bohr VA
541 (2010) The involvement of human RECQL4 in DNA double-strand break repair. *Aging Cell* **9**: 358-371.

542 Smeets MF, DeLuca E, Wall M, Quach JM, Chalk AM, Deans AJ, Heierhorst J, Purton LE, Izon DJ &
543 Walkley CR (2014) The Rothmund-Thomson syndrome helicase RECQL4 is essential for hematopoiesis.
544 *The Journal of Clinical Investigation* **124**: 3551-3565.

545 Svandova E, Anthwal N, Tucker AS & Matalova E (2020) Diverse Fate of an Enigmatic Structure: 200
546 Years of Meckel's Cartilage. *Front Cell Dev Biol* **8**: 821.

547 Van Maldergem L, Piard J, Larizza L & Wang LL (2007) Baller Gerold Syndrome. *GeneReviews,*(P. AM, J.
548 F & M. MG, eds.), p.^pp. University of Washington, Seattle, WA, USA.

549 Van Maldergem L, Piard J, Larizza L & Wang LL (2016) 1141RECQL4-Related Recessive Conditions.
550 *Epstein's Inborn Errors of Development: The Molecular Basis of Clinical Disorders of*
551 *Morphogenesis,*(Erickson RP & Wynshaw-Boris AJ, eds.), p.^pp. 0. Oxford University Press.

552 Van Maldergem L, Siitonen HA, Jalkh N*, et al.* (2006) Revisiting the craniosynostosis-radial ray
553 hypoplasia association: Baller-Gerold syndrome caused by mutations in the RECQL4 gene. *J Med Genet*
554 **43**: 148-152.

555 Vargesson N & Hootnick DR (2017) Arterial dysgenesis and limb defects: Clinical and experimental
556 examples. *Reprod Toxicol* **70**: 21-29.

557 Walls JR, Coultas L, Rossant J & Henkelman RM (2008) Three-dimensional analysis of vascular
558 development in the mouse embryo. *PLoS One* **3**: e2853.

Wang LL & Plon SE (1999) Rothmund-Thomson Syndrome. *Gene Reviews,*(P. AM, J. F & M. MG, eds.), p.^pp. University of Washington, Seattle, WA, USA.

Wang LL, Gannavarapu A, Kozinetz CA*, et al.* (2003) Association between osteosarcoma and deleterious mutations in the RECQL4 gene in Rothmund-Thomson syndrome. *J Natl Cancer Inst* **95**: 669-674.

Willsey HR, Seaby EG, Godwin A, Ennis S, Guille M & Grainger RM (2024) Modelling human genetic disorders in Xenopus tropicalis. *Dis Model Mech* **17**.

Willsey HR, Exner CRT, Xu Y*, et al.* (2021) Parallel in vivo analysis of large-effect autism genes implicates cortical neurogenesis and estrogen in risk and resilience. *Neuron* **109**: 1409.

Yadav S, Thakur S, Kohlhase J, Bhari N, Kabra M & Gupta N (2019) Report of Two Novel Mutations in Indian Patients with Rothmund-Thomson Syndrome. *J Pediatr Genet* **8**: 163-167.

Data availability statement:

All data are available in the main text or supplemental data file and videos are available via FigShare.

Supplementary data

Supplementary tables S1-S15 and Supplementary figures S1-S4 contain raw data and images and can be found in the attached supplementary data document. DOI for supplementary videos 1-3 hosted at Figshare are as follows:

Supplementary video 1: DOI 10.6084/m9.figshare.28640594

Supplementary video 2: DOI 10.6084/m9.figshare.28639817

Supplementary video 3: DOI 10 10.6084/m9.figshare.28640423